Heat transfer in aluminum-steel joint and weld tool during the friction stir welding: Simulation and experimental validation

Wenmin Ou (ouwenmin@cslg.edu.cn)
Changshu Institute of Technology
Guolin Guo
Chenshuo Cui
Yaocheng Zhang
Longgen Qian

Research Article

Keywords: Heat transfer, Friction stir welding, Aluminum-Steel joint, Weld tool

Posted Date: June 13th, 2022

DOI: https://doi.org/10.21203/rs.3.rs-1717755/v1

Heat transfer in aluminum-steel joint and weld tool during the friction stir welding: Simulation and experimental validation

Wenmin Ou[1,*], Guolin Guo[1], Chenshuo Cui[1], Yaocheng Zhang[1], Longgen Qian[2]

(1 School of Automotive Engineering, Changshu Institute of Technology, Changshu 215500, China

2 School of Mechanical Engineering, Changshu Institute of Technology, Changshu 215500, China)

* Corresponding author. E-mail address: ouwenmin@cslg.edu.cn

(Wenmin Ou)

Abstract: The heat transfer behaviors are important to control the performance of Aluminum-Steel joint. However, because the models with weld tool are majorly tested for the same material joints, the heat transfer behaviors with weld tool for aluminum-steel joint are not fully understood. In this paper, a novel CFD model with weld tool is developed and tested to investigate the effects of weld tool on the aluminum-steel joint. The calculated temperature and thermal cycles for various traverse speed agreed well with the corresponding IR experimental results. It is found that the model with weld tool can decrease the temperature gradient and inhomogeneity of temperature field for aluminum-steel joint. The model with weld tool can provide calculated viscosity based on the validated

temperature field to analysis the insufficient stirring defect of aluminum-steel joint.

Key Words: Heat transfer, Friction stir welding, Aluminum-Steel joint, Weld tool

1. Introduction

Aluminum-steel composite structure can meet the industrial requirements of structural performance and lightweight design [1]. Therefore, joining of aluminum to steel is of increasing interest for a wide range of industrial applications [2]. The heat transfer controls aluminum-steel joint performance. If joining method is fusion weld, the peak temperature exceeds the melting point, so brittle intermetallic compounds (IMCs) are formed resulting in poor joint performance [3]. Friction stir welding (FSW) is solid state joining method which indicated the peak temperature is much lower than the melting point, so it can restrict the generation of IMCs [2]. S. Bozzi et al. investigated the interface Al 6016/IF-steel in friction stir welding spots, it is found that the thickness of IMCs layer can be restricted by decreasing heat flux in tool pin [4]. L. Wan et al. reviewed friction stir welding (FSW) of dissimilar aluminum alloys and steels, it is generally believed that the thickness of IMCs layer increases with the increase of heat input during the FSW process [5]. H. Aghajani Derazkola et al. verified the Arrhenius relations between the

thickness of the IMCs layer and the temperature in the butt joints of AA5005-O aluminum-magnesium alloy and St-52 low carbon steel sheets [6].

Therefore，thickness of IMCs layer is depend on the heat transfer during FSW. In order to control the heat transfer to obtain sound joints, special tools are designed including cutting pin with rotary burrs [7], tool with scribe made of tungsten carbide-cobalt cermet [8] and scrolled tool with scribe affixed to pin tip [9]. etc. However, large differences in their thermal properties such as expansion coefficient, conductivity, and specific heat can lead to defect. Understanding the effects of tool on the heat transfer behaviors in friction stir welding is of great significance for producing free defect joints based on scientific principles. Owing to interaction between thermal and machinal and the complex profile between the tool and workpiece, the heat transfer behaviors with tool are complicated and not fully understood [10]. Because of the difficulties in experimentally measuring the temperature in the vicinity of the welding tool, the numerical analysis has been generally employed in investigating the effects of the welding tool on heat transfer behavior [11~13].

The numerical model to consider the weld tool is more precise but more difficult. Su et al. established the numerical models with two tools of different pin shapes (axisymmetrical conical tool and asymmetrical triflat tool) [14]. In order to obtain higher precise in their model, the boundary

conditions of heat transfer and material flow are determined with considering a partial sticking/sliding contact condition at the tool–workpiece interface. Sun et al. developed the numerical model with weld tool to analyze the influence of tool thread pitch on the material flow and thermal process in FSW [15]. Their results shows that the total heat generation decreases with increase in thread pitch, which may not be measured in experiments. Chen et al. [16] also investigated the influent of pin thread on the material flow and thermal process. Comparing with Sun's model, their model is more complicated, the transient rotation of the threaded pin is implemented explicitly via fully transient control of the zone motion. Chen et al. [17] further compared the boundary velocity (BV) models and the boundary shear stress (BSS) models to analyze the heat transfer and plastic deformation behaviors during the FSW of AA2024. It indicated that different boundary conditions yield similar predictions on temperature, but quite different predictions on material deformation. These fine models provide detail technical information about setting boundary conditions and calculation zones, but they didn't provide detail information about heat transfer in weld tool. In later studies, by developing coupled thermomechanical model [18-19] and retractable pin tool FSW model without heat transfer in weld tool [20], it was generally noted that heat transfer between the welding tool and the workpiece can be applied to predict the heat generation and recrystallized grain. B.Aziz et al.

investigated the heat generation by considering heat transfer in weld tool [21]. The simulation results showed that the highest relative error is below 6% by comparing simulated temperature profile of three different weld schedules. Miles et al. reported more precise result to predict recrystallized grain by considering heat transfer in weld tool [22]. It also showed that the heat generated during FSW was predicted to within 5% of the experiment. Mirabzadeh et al. developed a 3-D symmetric Finite Element (FE) model to estimate the generated and distributed heat for polypropylene sheet joints [23]. It indicated that if the heat transfer in weld tool is well predicted, the number of experiment tests may be reduced. However, these models are only tested for the same material joints, the application of the model with weld tool for aluminum-steel joints was quite limited. H. Aghajani Derazkola et al. developed and tested computational fluid dynamics (CFD) model without weld tool for aluminum-steel joints in underwater environment [24]. However, the model with weld tool capable of calculating the heat transfer for aluminum-steel joints is also not well-tested.

In this paper, there dimension model with weld tool is developed to calculate the heat transfer and material flow of aluminum-steel joint based on CFD. Since the FSW system is consists of aluminum, steel, weld tool head and weld tool pin, the calculation zone is also divided into four parts. The boundary conditions are carefully set, especially at the tool/workpiece

interface. The simulation results are validated by conducting infrared (IR) thermography experiments at different traverse speed. The effects of tool on heat transfer in the friction stir welding of aluminum-steel joint are discussed.

2. Experiment

Friction stir butt joining of 6061 aluminum alloy and 304 stainless steel was carried out in this study. The dimensions of each workpiece were 150 mm×75 mm × 3 mm (length × width × thickness). The welding tool was made of the H13 steel. The welding tool shoulder was 18 mm in diameter, and length of the pin was 2.7 mm. The pin had a conical geometry. The diameter of pin was 7 mm near the shoulder and 5 mm at the tip.

A schematic view of the FSW system is illustrated in Fig. 1. Two kinds of IR cameras are used in the system, one is Optris PI-20072263 with measured temperature range from 293 K to 1173 K, the other is Optris PI-20032134 with measured temperature range from 723 K to 2073 K. The FSW equipment is developed from Computerized Numerical Control (CNC) machine tool. The 3 axis independent movements of the machine tool are programed and controlled by a software-based control system. The employed plunge depth was 0 mm, and no tilt angle was adopted. The steel is set on advancing side (AS) and the aluminum is set on retreating side (RS) [25]. In the welding process, welding direction is along the length of workpiece and the workpiece traverse speed is the controlled variable. The

welding parameters are shown in Table 1.

Table 1 FSW process parameters of test cases

Test case	Traverse speed (mm/min)	Rotated speed (r/min)	Tool offset (mm)
1#	40	800	0
2#	50	800	0
3#	60	800	0
4#	70	800	0
5#	80	800	0

The specimens for examination of the cross-sectional macrostructure were grounded, polished and etched with different solution due to dissimilar material. Firstly, the 304 stainless steel was etched with concentrated aqua regia solution (30 mL hydrochloric acid and 10 mL nitric acid) for 15 s and then the 6061 aluminum alloy was etched with Keller's solution (95 mL water, 1.5 mL hydrochloric acid, 2.5 mL nitric acid, 1 ml hydrofluoric acid) for 60 s. After that, the cross-sectional macrostructure of specimens was observed by optical microscopy.

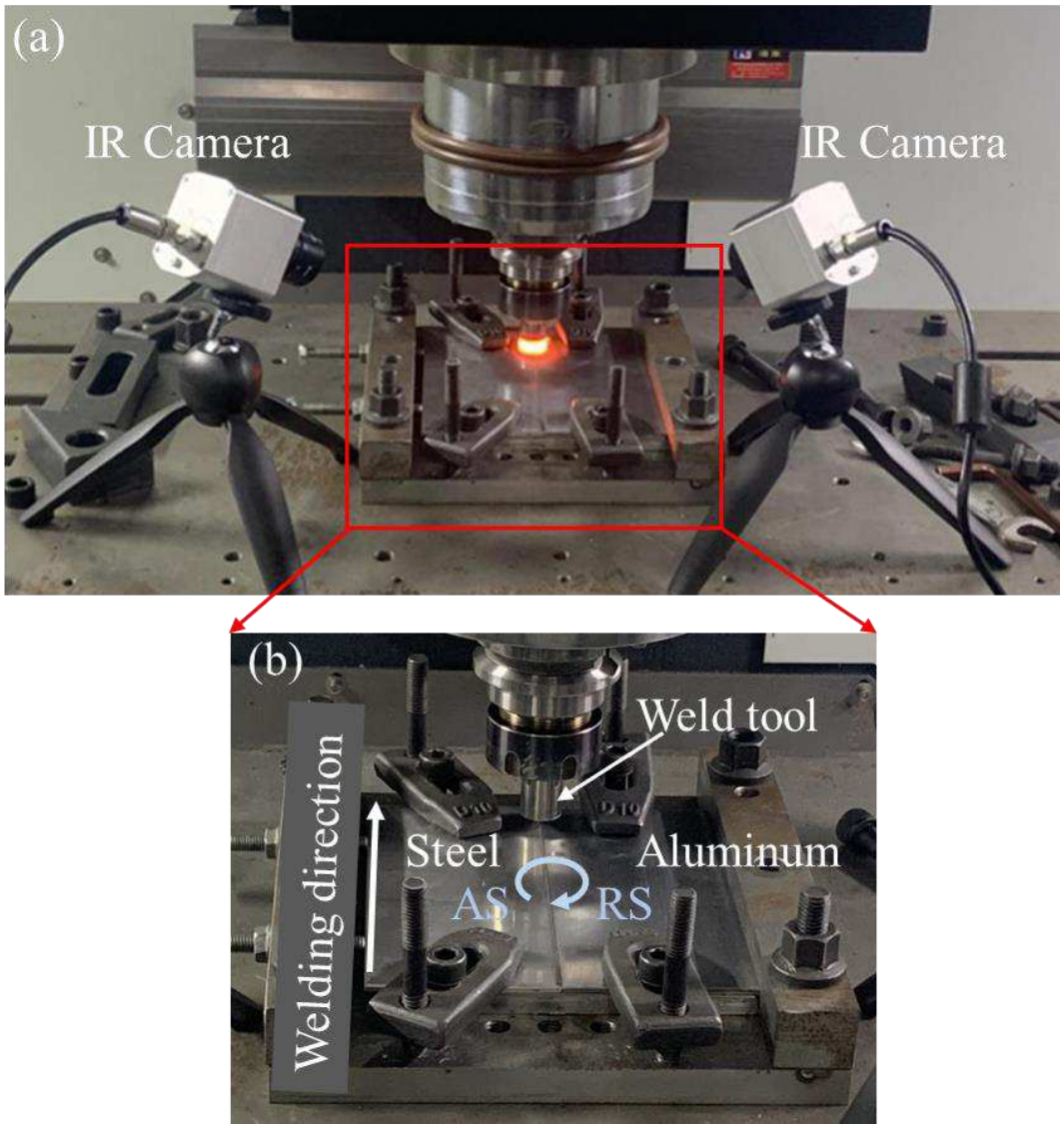

Fig. 1. The FSW equipment for aluminum-steel joint. (a) The system included IR camera to measure the temperature. (b) Magnified views of workpiece and clamp in (a).

3. Numerical model

3.1 Assumptions

The following simplifying assumptions are made to make the numerical calculations involving heat and material flow tractable.

(1) Comparing with fusion weld, the temperature is below the melting

point during FSW, so the thermal properties parameters are assumed to be constant, but the viscosity of the material varied with temperature.

(2) The FSW process is assumed to be quasi-steady state, while the highly transient process at the beginning and end of welding are ignored.

3.2 Governing equations

The conservation equations of mass, momentum and energy were solved, using the commercial package, ANSYS Fluent [26]. The steady-state continuity equation, momentum conservation equations and energy equation for incompressible multi-phase flow were given by [24]:

$$\nabla \cdot (\bar{\rho}\vec{v}) = 0$$

$$\nabla \cdot (\bar{\rho}\vec{v}\vec{v}) = -\nabla \mathrm{p} + \nabla \cdot (\bar{\mu}\nabla\vec{v}) - \nabla \cdot \left(\bar{\rho}\vec{U}\vec{v}\right) \quad (2)$$

$$\nabla \cdot (\bar{\rho}\vec{v}H) = \nabla \cdot \left(\frac{\bar{k}}{\bar{C}_P}\nabla H\right) - \nabla \cdot \left(\bar{\rho}\vec{U}H\right) + S_v \quad (3)$$

$$\bar{\rho} = \sum_{i=1}^{2} \Omega_i \rho_i$$

$$\bar{\mu} = \sum_{i=1}^{2} \Omega_i \mu_i$$

$\bar{k}$

$$= \sum_{i=1}^{2} \Omega_i k_i$$

$\bar{C}_P$

$$= \sum_{i=1}^{2} \Omega_i C_{Pi}$$

Where $\bar{\rho}$ is the mix density, $\bar{\mu}$ is the mix non-Newtonian viscosity, p is the pressure, $\vec{v}$ is the velocity of material flow, $\vec{U}$ is the welding velocity, H is the total enthalpy of the material, $\bar{k}$ is the mix thermal conductivity and $\bar{C}_P$ is the mix specific heat. S_v is the viscous dissipation heat generation due to plastic material flow originated by high strain rate inside the shear zone of the workpiece near the tool. Ω_i is the volume fraction of each phase. ρ_i is the density of *i* phase. μ_i is the non-Newtonian viscosity of *i* phase. k_i is the thermal conductivity of *i* phase. C_{Pi} is the specific heat of *i* phase.

3.3. Calculation zones and boundary conditions

In order to simulate the heat transfer for aluminum-steel joint, the calculation zones should be set firstly. In this paper, the whole domain is divided into four calculation zones including steel zone, aluminum zone, weld tool head zone and weld tool pin zone as shown in fig. 2.

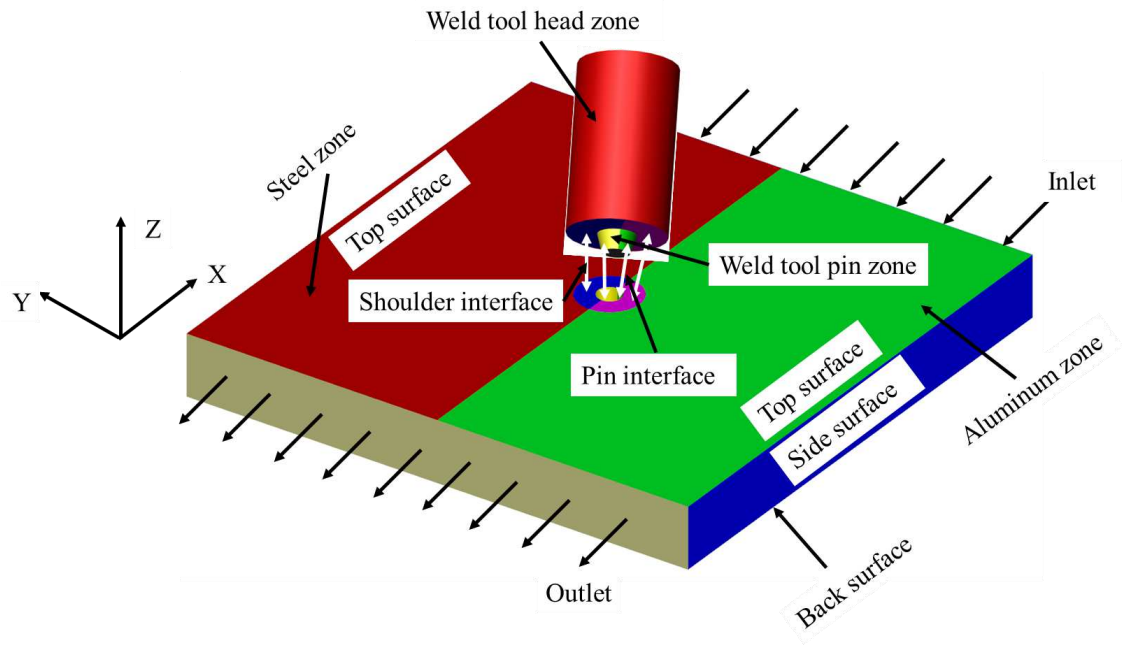

Fig. 2. Schematic of the calculation zones and boundary positions consisting of weld tool and workpiece.

The model has nigh kinds of boundaries corresponding with each calculation zone, as listed in Table 2. In this model, material flows into and out the computational domain through the 'Inlet' and 'Outlet' boundary with same speed in the experiment. The translational momentum boundary indicates the surface moves with same speed corresponding to the weld parameters list in table 1, so as well as the rotational momentum boundary. In terms to the thermal boundary, the type of 'Inlet' and 'Outlet' is temperature which equal to the ambient temperature 300K. The heat transfer is convection at the 'Top surface', 'Back surface' and 'Side surface', the corresponding heat transfer coefficient are estimated as 30 W/m^2-K [27], 800 W/ m^2-K [28] and 800 W/ m^2-K [28] respectively. Frictional heat will be generated on the 'Shoulder interface', 'Pin interface'

and ‘Pin bottom’ boundaries, the calculation equations will be given in the section of heat generation. No heat generation is assumed at the ‘Tool head side’ boundary, so the heat flux is set as 0 W/m^2.

Table 2 Boundary conditions in the models.

Boundary	Type	Momentum	Thermal
Inlet	Velocity inlet	Translational	Temperature (300 K)
Outlet	Velocity outlet	Translational	Temperature (300 K)
Top surface	Wall (No Slip)	Translational	Convection (30 W/m^2-K)
Back surface	Wall (No Slip)	Translational	Convection (800 W/m^2-K)
Side surface	Wall (No Slip)	Translational	Convection (800 W/m^2-K)
Shoulder interface	Wall (No Slip)	Rotational	Coupled (Heat generation)
Pin interface	Wall (No Slip)	Rotational	Coupled (Heat generation)
Pin bottom	Wall (No Slip)	Rotational	Coupled (Heat generation)
Tool head side	Wall (No Slip)	Rotational	Heat flux (0 W/m^2)

Fig. 3 shows the mesh of the geometry model. The model contains 128,667 mixed cells of steel zone, 128,673 mixed cells of aluminum zone, 4600 hexahedral cells of weld tool head zone and 468 hexahedral cells of weld tool pin zone. In order to obtain the accurate distribution of heat flux and reduce the calculation time, a smaller mesh size is applied in the vicinity of the welding tool and the mesh size gradually increases with the increase of the radial distance. The maximum and minimum volume of hexahedral cells in the model are 2.21×10^{-9} m^3 and 1.82×10^{-11} m^3

respectively.

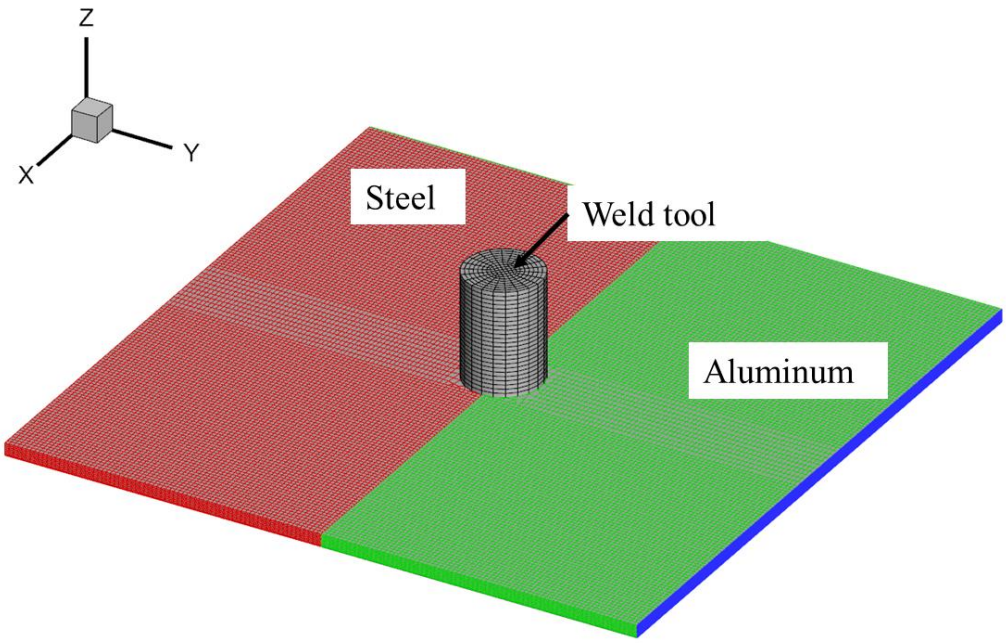

Fig. 3. The mesh of aluminum-steel joint and weld tool.

3.4. Material properties

The materials of joint and weld tool are dissimilar, so the thermo-physical properties should be loaded to the corresponding calculation zone. The thermophysical properties of the alloys are provided in Table 3 [29,30].

Table 3 Thermophysical properties of 304 stainless steel, 6061 aluminum alloy and H13 steel [29,30].

Properties	304	6061	H13
Density (Kg/m^3)	7800	2705	7800
Specific heat (J/kg-K)	520	850	734.3
Thermal conductivity (W/m-K)	24	210	30.4

The viscosity is important for material flow and hat generation, so it is determined by the below formula based on the theory of visco-plasticity

[31]:

$$\mu = \frac{\sigma}{3\dot{\varepsilon}} \tag{8}$$

Where σ is flow stress of the workpiece and $\dot{\varepsilon}$ is the effective strain rate, which is defined by:

$$\dot{\varepsilon} = \sqrt{\frac{2}{3}\dot{\varepsilon_{ij}}\dot{\varepsilon_{ij}}} \tag{9}$$

Where $\dot{\varepsilon_{ij}}$ is the strain rate tensor given by:

$$\dot{\varepsilon_{ij}} = \frac{1}{2}\left(\frac{\partial v_i}{\partial x_j} + \frac{\partial v_j}{\partial x_i}\right) \tag{10}$$

The detail calculation of strain rate can be found in Appendix A of reference [32].

Flow stress of the workpiece is considered to be temperature and strain rate dependent and can be obtained through formula (7~8) [33]:

$$\sigma = \frac{1}{\alpha} ln\left\{\left(\frac{Z}{A}\right)^{1/n} + \left[1 + \left(\frac{Z}{A}\right)^{2/n}\right]^{1/2}\right\} \tag{11}$$

$$Z = \dot{\varepsilon} exp\left(\frac{Q}{RT}\right) \tag{12}$$

Where T is temperature obtained from energy equation (3), A (s^{-1}) and n are material constants, Q is the thermal deformation activation energy, R is the ideal gas constant. These parameters can be found in the Table 3 of literature [34].

3.5. Heat generation

The heat generation during FSW is consists of plastic deformation and the friction at the welding tool/workpiece interface. The plastic

deformation heat is taken into source item S_v in energy equation (3), which is defined by:

$$S_v = \mathrm{K} \cdot \sigma \cdot \dot{\varepsilon} \qquad (13)$$

Where K =0.6 [3] is the mechanical efficiency.

The heat generated at the welding tool/workpiece interface is set in the boundary conditions. The interfacial friction heat is given as follow.

$$q_f = \eta \left\| \overrightarrow{\tau_f} \right\| \left\| \overrightarrow{V_{vel}} \right\| \qquad (14)$$

Where η is the ratio of the heat absorbed by the workpiece, which is 0.6 for aluminum alloy and 0.4 for stainless steel; $\overrightarrow{\tau_f}$ is the frictional tangential force and $\overrightarrow{V_{vel}}$ is the relative velocity between the welding tool and the workpiece. The magnitude of these vectors can be calculated from the reference [35]. It should be note that the thermal boundary condition type of the tool/workpiece interface is couple, which assumed heat continuously transfer between the different calculation zones through a very thin wall. The thickness of thin wall in this study is set as 0.01 mm, and the heat generation rate is given as follow.

$$Q_f = \frac{q_f}{a} \qquad (15)$$

Where Q_f (W/m^3) is the heat generation rate at the welding tool/workpiece interface, a is the thickness of thin wall.

4. Results and discussion

4.1. Predicted the temperature and material flow

Fig. 4 shows the temperature field in the weld tool. It is obviously

found that the temperature field is asymmetric due to the different thermophysical properties of dissimilar materials at the shoulder interface. Because stainless steel at AS has much lower thermal conductivity, the temperature significantly decreases with increasing radius, which indicates larger inhomogeneity of temperature field at AS. In contrast, the aluminum alloy has higher thermal conductivity, so the smaller inhomogeneity of temperature field at RS is observed. Similarly, the peak temperature of AS is above 520 K, which is about 100 K higher than that of RS. Because the size of pin interface is smaller, the inhomogeneity of temperature field at pin interface is not so significant. However, it has the same law as shoulder interface. The temperature of weld tool head decreases with increasing length along Z direction.

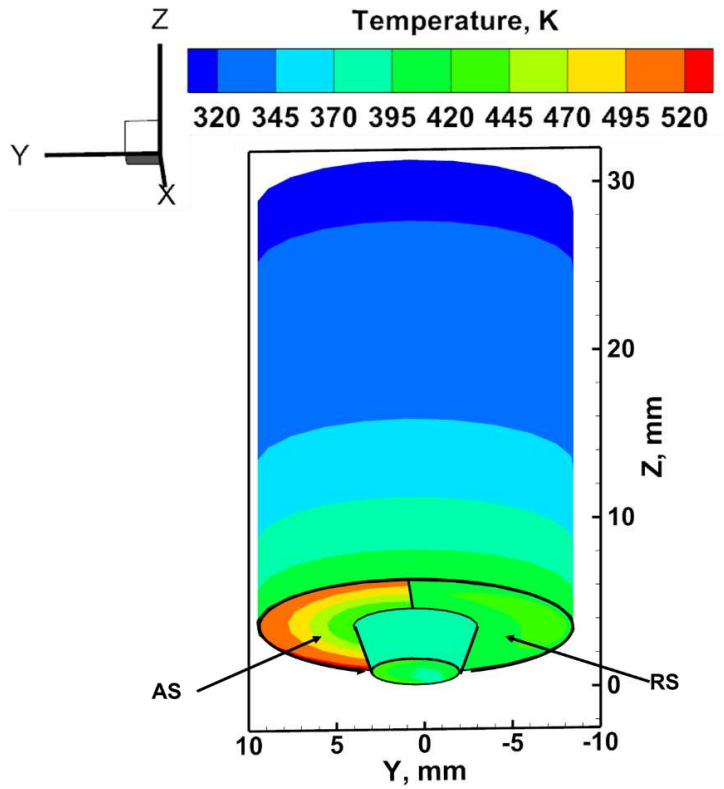

Fig. 4. The temperature field in the weld tool at traverse speed 40 mm/min.

The other parameters are given in table 1.

Fig. 5 shows the temperature field in the workpiece. It is found that the temperature field is corresponded with weld tool due to the coupled boundary condition at the shoulder interface. This indicates that the thickness of thin wall assumption works in the equation (15). In the workpiece, it is observed that the temperature field diffused at different velocity, which is measured by diffusion coefficient λ shown as below.

$$\lambda = \frac{k}{C_P} \tag{16}$$

Substituting the thermal conductivity and specific heat in the table 3, the thermal diffusion coefficient of stainless steel is 0.046 and aluminum alloy is 0.247. The diffusion coefficient of aluminum alloy is about 5 times that of steel, so the diffusion width of the temperature field on the RS is much larger than that on the AS.

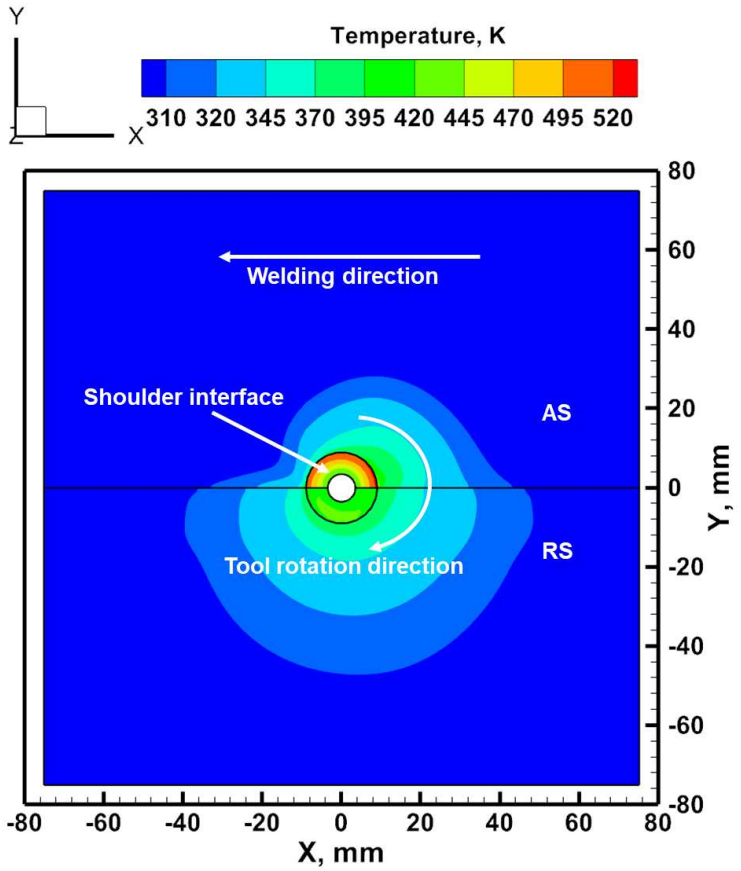

Fig. 5. The temperature field in the workpiece at traverse speed 40 mm/min. The other parameters are given in table 1.

Fig. 6 shows the material flow in the weld tool head and workpiece. The weld tool head rotates without the influence of the workpiece, so it has the maximum velocity, which is same with rotated speed. Near the tool/workpiece interface, the material flows slightly slower than the weld tool head. Because the viscosity of plastic stainless steel is higher than plastic aluminum alloy, the material flows slightly faster in RS.

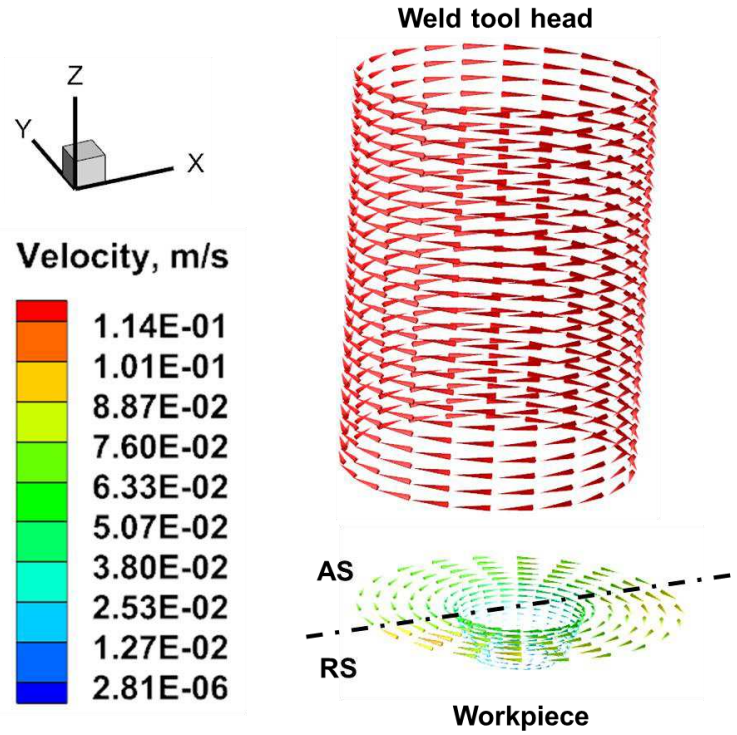

Fig. 6. The material flow in the weld tool and workpiece at traverse speed 40 mm/min. The other parameters are given in table 1.

4.2. Validation the temperature filed of aluminum-steel joint

The temperature during FSW process is measured by IR camera. Fig. 7 shows the measured temperature field of test case 1, three points in the workpiece and weld tool head are selected to validate the calculation accuracy of the model. The locations of measured points are quantitative by distance from the reference lines as shown in Fig. 7(c), so the temperature can be capture in experiments and numerical model.

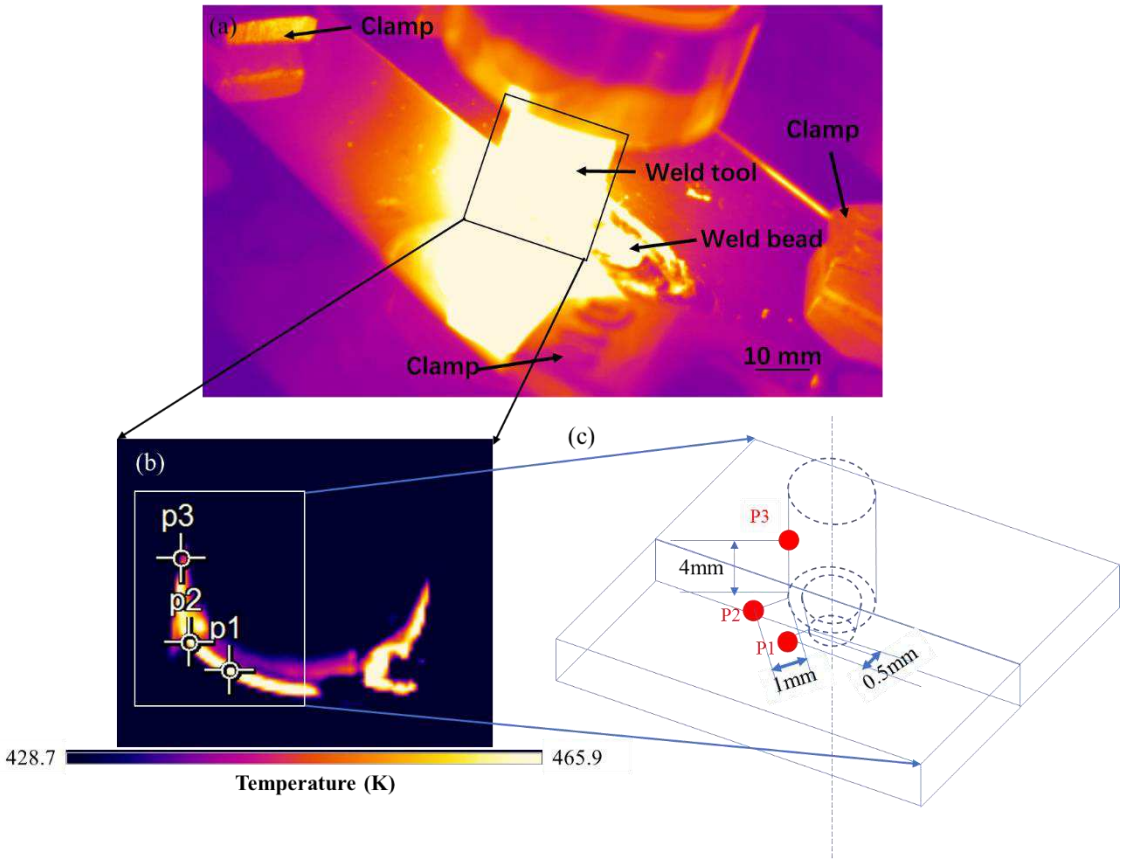

Fig. 7. (a) The measured temperature field of test case 1. (b) three points 'p1', 'p2' and 'p3' are selected to validate the model by comparing calculated results and measured results. (c) the distance of measured points in the workpiece and weld tool.

The calculation temperature and relative error are list in table 4. It is found that the temperature decreases with increasing height along the weld tool, which is consistent with simulation result. The relative error is smaller than 10%, which indicates that the calculation accuracy is accepted. The relative error is higher near the shoulder interface due to the complex thermo-mechanical processes.

Table 4 Comparisons results between measured and calculated temperature of three monitor points along the weld tool

Points	Measured Temperature (K)	Calculated Temperature (K)	Relative Error
p1	492.3	446.2	9.4%
p2	475.1	435.6	8.3%
p3	439.4	406.3	7.5%

The thermal cycle curve plays an important role in determining weld joint microstructure, properties and performance. Fig. 8 shows the measured point at different traverse speed is adopted to validate the thermal cycle. Because the relative error near the shoulder interface is higher, the measured point is set as 10 mm distance from the joint center. The flash is observed during experiments. Although, the temperature of flash can be measured by IR camera, it can’t be considered in this model. This is one of the error sources of thermal cycle.

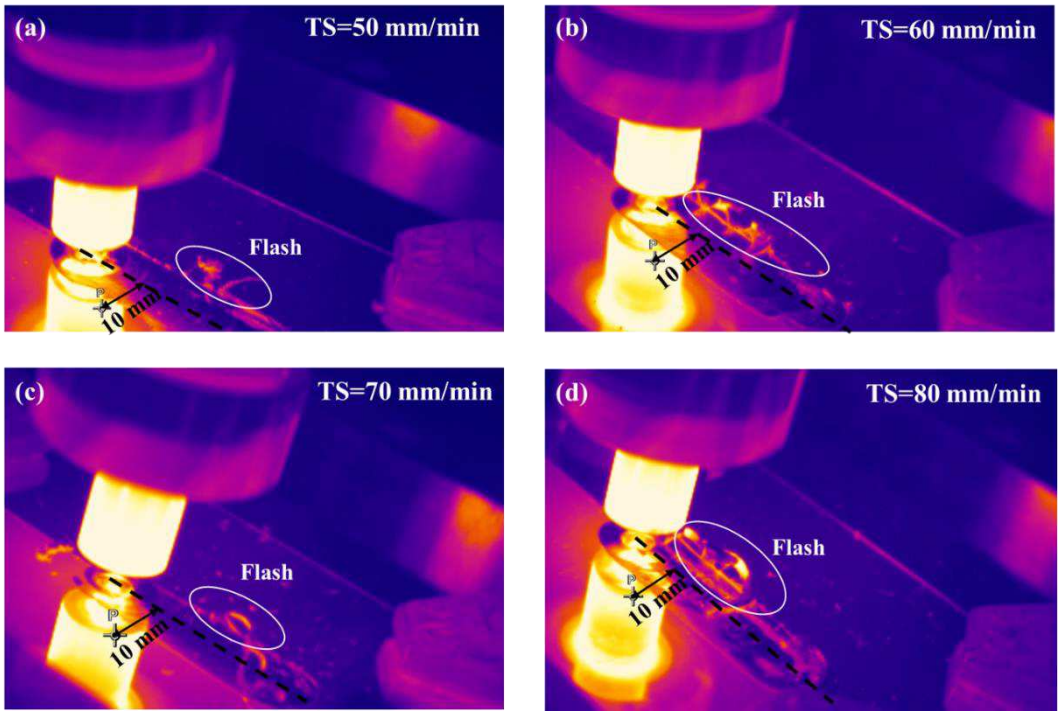

Fig. 8. The typical temperature field distribution during FSW by the IR camera. 'TS' means the different traverse speed. (a) at traverse speed 50 mm/min (b) at traverse speed 60 mm/min (c) at traverse speed 70 mm/min (d) at traverse speed 80 mm/min. The other parameters are given in table 1.

Since the quasi-steady state assumption is adopted in this model, the thermal cycle can be calculated based on the equation (16) in reference [36]. The comparison results between experiment and calculation are shown in Fig. 9. It is found that the calculation peak temperature is slightly lower than experiment. The heating rate of calculation thermal cycle is slightly delay during heat stage. The cooling rate of calculation is better matching with experiments. However, it seems that the relative error of cooling stage increases with increasing traverse speed.

The agreement of the calculated temperature at measured point (Table 4), as well as agreement of thermal cycles for various traverse speed (Fig. 9) with corresponding experimental data provides confidence in using the model to investigate the effects of weld tool on temperature field.

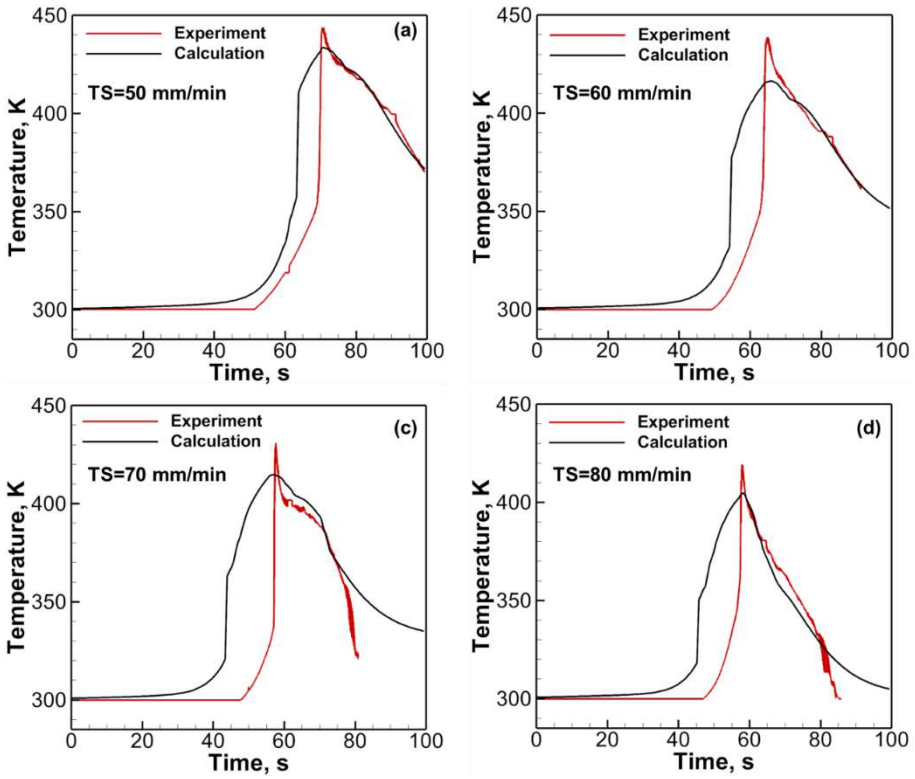

Fig. 9. Comparison between the calculated and the experimentally measured thermal cycles at different traverse speed. (a) at traverse speed 50 mm/min (b) at traverse speed 60 mm/min (c) at traverse speed 70 mm/min (d) at traverse speed 80 mm/min. The other parameters are given in table 1.

4.3. Comparison analysis of the effects of welding tool

Fig. 10 shows the comparison results of YZ cross sections between the model without weld tool and the model with weld tool. Because much more heat will transfer in the weld tool, it is obviously observed that much

less heat accumulated at AS in the model with weld tool. As the traverse speed accelerates, the temperature obviously decreases in the model with weld tool, but it slightly decreases in the model without weld tool. It indicates that the model with weld tool fits the experiment results better.

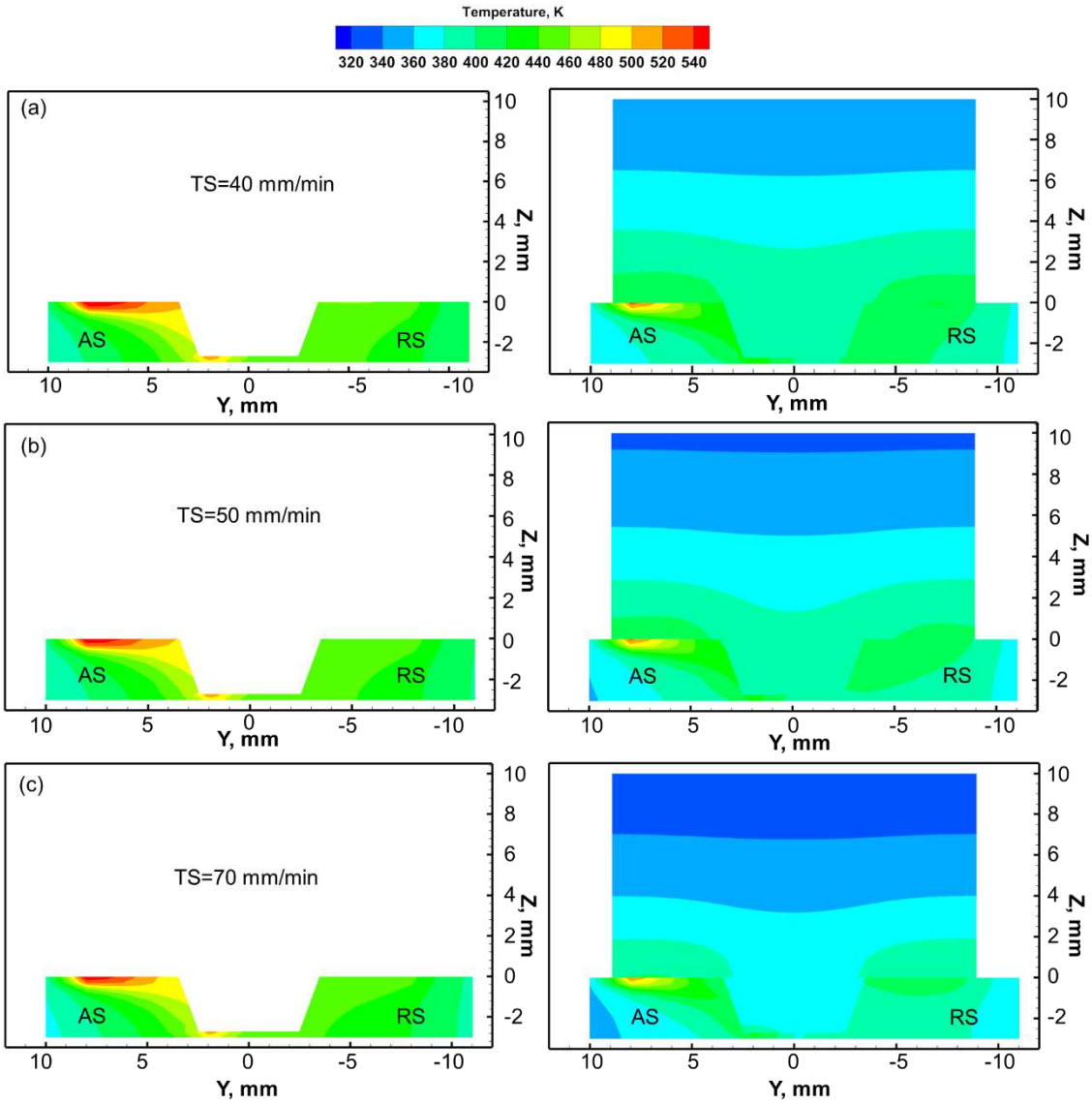

Fig. 10. Comparison temperature field on YZ cross sections between the model without weld tool and the model with weld tool at the corresponding traverse speed. (a) at traverse speed 40 mm/min (b) at traverse speed 50 mm/min (c) at traverse speed 70 mm/min.

Fig. 11 shows the comparison results of XY cross sections between the model without weld tool and the model with weld tool. It is observed that the higher temperature zone is larger at AS in the model without weld tool. In contrasts, the temperature gradient is lower in the model with weld tool. This is because the weld tool can also transfer heat, it reduces the temperature difference between AS and RS. The maximum temperature difference between AS and RS can be above 200 K in the model without weld tool, but this temperature difference is about 150 K in the model with weld tool. It indicates that the smaller inhomogeneity of temperature field is obtained by employing the model with weld tool.

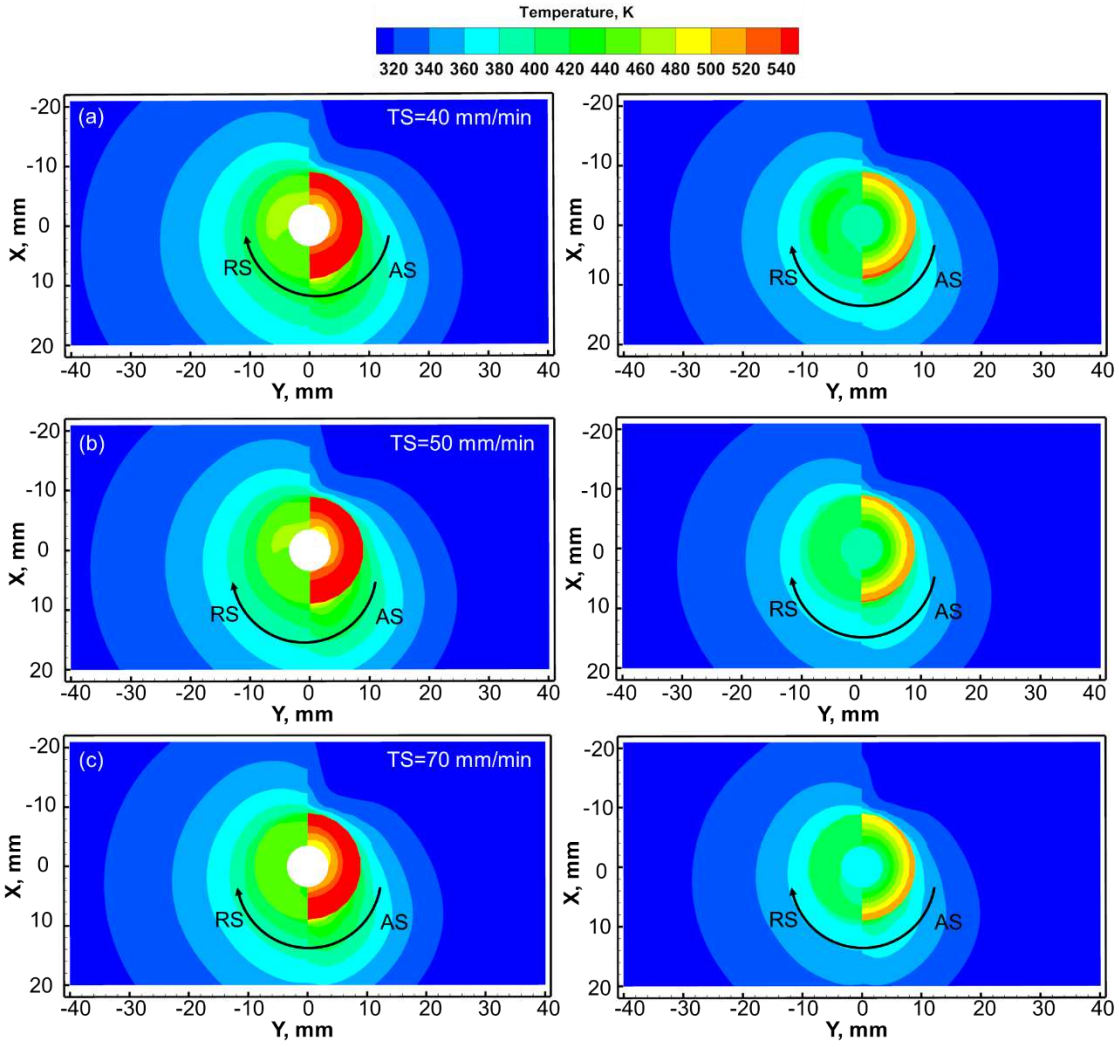

Fig. 11. Comparison temperature field on XY cross sections between the model without weld tool and the model with weld tool at the corresponding traverse speed. (a) at traverse speed 40 mm/min (b) at traverse speed 50 mm/min (c) at traverse speed 70 mm/min.

The aluminum-steel joint is dissimilar material, so the temperature gradient is different at AS and RS. Fig. 12 shows the temperature gradient varied with traverse speed at AS and RS. If the traverse speed is same, the temperature gradient is about 30 K/mm larger at AS than that at RS. In additions, the temperature gradient is about 20 K/mm larger at AS and 5

K/mm larger at RS in the model without weld tool. As the traverse speed accelerates, the temperature gradient both decreases in the model without weld tool and the model with weld tool.

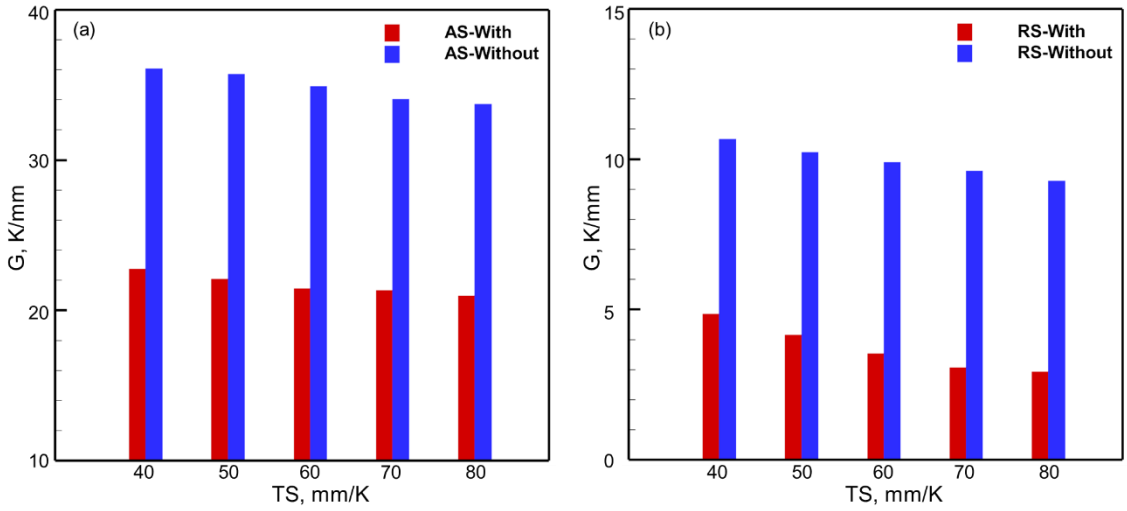

Fig. 12. Temperature gradient varied with traverse speed between the model without weld tool and the model with weld tool. (a) at AS, where 'AS-With' means the model with weld tool at AS, 'AS-Without' means the model without weld tool (b) at RS, where 'RS-With' means the model with weld tool at RS, 'RS-Without' means the model without weld tool. 'TS' indicates traverse speed and 'G' indicates the temperature gradient.

The large temperature difference and temperature gradient at AS and RS determine the relationship between macrostructure and viscosity. Fig. 13 shows the macrostructure and viscosity near the pin at two different traverse speed level. It is observed that the material is insufficient stirring at RS due to the different material viscosity. Although this kind of defect can't be simulated in this model, the model can provide calculated viscosity based on the temperature field as shown in Fig. 10. Since the significant

inhomogeneity of temperature field for aluminum-steel joint, the steel and aluminum viscosity can differ by an order of magnitude. As the traverse speed accelerated, the peak temperature and temperature difference between AS and RS decreased, so the plastic zones shrink at 70 mm/min traverse speed as shown in Fig. 13(d).

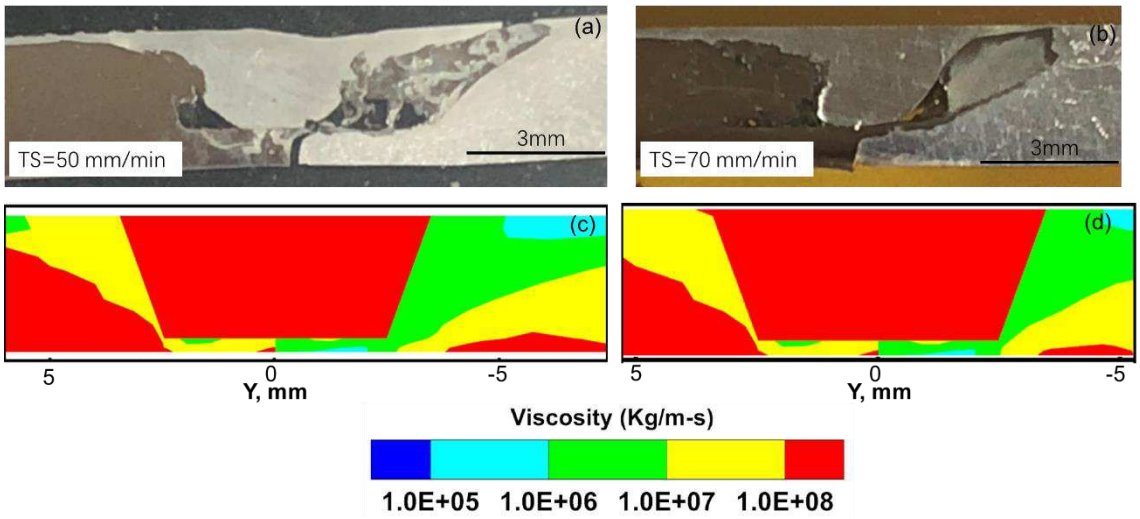

Fig. 13. The macrostructure of aluminum-steel joint at corresponding traverse speed (a) 50 mm/min (b) 70 mm/min. The calculated viscosity near the pin at corresponding traverse speed (c) 50 mm/min (d) 70 mm/min.

5. Conclusions

In this paper, a novel CFD model with weld tool is developed to investigate the effects of weld tool on the aluminum-steel joint. The following conclusions could be obtained:

(1) The calculated temperature and thermal cycles for various traverse speed agreed well with the corresponding IR experimental results. The relative error of monitor points is smaller than 10%, which indicates that the calculation accuracy is accepted.

(2) The inhomogeneity of heat generation and material flow is observed between AS and RS of aluminum-steel joint. The model with weld tool decreases the temperature gradient and inhomogeneity of temperature field for aluminum-steel joint to provide the more accurate prediction results.

(3) The viscosity can differ by an order of magnitude between steel and aluminum alloy. The model can provide calculated viscosity based on the temperature field to analysis the insufficient stirring defect.

Author contribution Wenmin Ou and Guolin Guo conceived and designed the study. Chenshuo Cui and Yaocheng Zhang performed the experiments. Longgen Qian and Wenin Ou established the model. Wenmin Ou and Guolin Guo reviewed and edited the manuscript. All the authors read and approved the manuscript.

Funding This work was supported by the Natural Science Fund for Colleges and Universities in Jiangsu Province (20KJB460013).

Availability of data and material The datasets generated and/or analyzed during the current study are available from the corresponding author on reasonable request.

Code availability The codes used to reproduce this work cannot be shared at this time as they are part of an ongoing study.

Declarations

Ethics approval Not applicable.

Consent to participate Not applicable

Consent for publication The author confirms that the work has not been published before; that it is not under consideration for publication elsewhere that its publication has been approved by all co-authors; that its publication has been approved by the responsible authorities at the institution where the work is carried out.

Competing interests The authors declare no competing interests.

References

[1] E. Taban, J. E.Gould, J. C.Lippold, Dissimilar friction welding of 6061-T6 aluminum and AISI 1018 steel: Properties and microstructural characterization, Materials & Design (1980-2015). 31 (5) (2010) 2305-2311.

[2] S.A. Hussein, A.S. Md Tahir, A.B. Hadzley, Characteristics of aluminum-to-steel joint made by friction stir welding: A review, Materials Today Communications. 5 (2015) 32-49.

[3] A. Heidarzadeh, S. Mironov , R. Kaibyshev, et al., Friction stir welding/processing of metals and alloys: A comprehensive review on

microstructural evolution, Progress in Materials Science, 117 (2021) 100752.

[4] S. Bozzi, A.L. Helbert-Etter, T. Baudin, et al., Intermetallic compounds in Al 6016/IF-steel friction stir spot welds[J]. Materials Science and Engineering: A, 2010, 527 (16-17): 4505-4509.

[5] L. Wan, Y. Huang. Friction stir welding of dissimilar aluminum alloys and steels: a review[J]. The International Journal of Advanced Manufacturing Technology, 2018, 99(5): 1781-1811.

[6] H. Aghajani Derazkola, F. Khodabakhshi. Intermetallic compounds (IMCs) formation during dissimilar friction-stir welding of AA5005 aluminum alloy to St-52 steel: numerical modeling and experimental study[J]. The International Journal of Advanced Manufacturing Technology, 2019, 100(9): 2401-2422.

[7] J.T. Xiong, J.L. Li, J.W. Qian, et al., High strength lap joint of aluminium and stainless steels fabricated by friction stir welding with cutting pin, Science & Technology of Welding & Joining, 17 (3) (2012) 196-201.

[8] T.H. Wang, H. Sidhar, R. S.Mishra, et al., Friction stir scribe welding technique for dissimilar joining of aluminium and galvanised steel, Science and Technology of Welding & Joining, 23 (2017) 1-7.

[9] E. E.Patterson, Y. Hovanski, D. P.Field, Microstructural Characterization of Friction Stir Welded Aluminum-Steel Joints,

Metallurgical & Materials Transactions A, 47 (6) (2016) 2815-2829.

[10] R. Rai, A. De, H. Bhadeshia, et al., friction stir welding tools[J]. Science and Technology of welding and Joining, 2011, 16 (4): 325-342.

[11] R. Nandan, T. Debroy, H. Bhadeshia, Recent advances in friction-stir welding – Process, weldment structure and properties, Progress in Materials Science, 53 (6) (2008) 980-1023.

[12] X.C. He, F.S. Gu, A. Ball, A Review of Numerical Analysis of Friction Stir Welding, Progress in Materials Science, 65(10) (2014) 1-66.

[13] D.M. Neto, P. Neto, Numerical modeling of friction stir welding process: a literature review, International Journal of Advanced Manufacturing Technology, 65 (1) (2013) 115-126.

[14] H. Su, C.S. Wu, M. Bachmann, et al., Numerical modeling for the effect of pin profiles on thermal and material flow characteristics in friction stir welding, Materials and Design, 77 (15) (2015) 114-125.

[15] Z. Sun, C.S. Wu, Influence of tool thread pitch on material flow and thermal process in friction stir welding, Journal of Materials Processing Technology, 275 (2020) 116281.

[16] G.Q. Chen, H. Li, G.Q. Wang, et al., Effects of pin thread on the in-process material flow behavior during friction stir welding: A computational fluid dynamics study, International Journal of Machine Tools and Manufacture, 124 (2018) 12-21.

[17] G.Q. Chen, Q.X. Ma, S. Zhang, et al., Computational fluid

dynamics simulation of friction stir welding:A comparative study on different frictional boundary conditions, Journal of Materials Science & Technology, 34 (1) (2018) 128-134.

[18] S. B.Aziz, M. W.Dewan, D. J.Huggett, et al., A Fully Coupled Thermomechanical Model of Friction Stir Welding(FSW) and Numerical Studies on Process Parameters of Lightweight Aluminum Alloy Joints, Acta Metallurgica Sinica (English Letters), 31 (2018) 1-18.

[19] N. Dialami, M. Chiumenti, M. Cervera, et al., Enhanced friction model for Friction Stir Welding (FSW) analysis: Simulation and experimental validation, International Journal of Mechanical Sciences, 133 (2017) 555-567.

[20] G.Q. Chen, G.Q. Wang, Q.Y. Shi, et al., Three-dimensional thermal-mechanical analysis of retractable pin tool friction stir welding process, Journal of Manufacturing Processes, 41 (2019) 1-9.

[21] S. B.Aziz, M. W.Dewan, D. J.Huggett, et al., Impact of Friction Stir Welding (FSW) Process Parameters on Thermal Modeling and Heat Generation of Aluminum Alloy Joints[J]. Acta Metallurgica Sinica, 2016, 29(9):1-15.

[22] M.P. Miles, T.W. Nelson, C. Gunter, et al., Predicting recrystallized grain size in friction stir processed 304L stainless steel, Journal of Materials Science & Technology, 35(04) (2019) 491-498.

[23] R. Mirabzadeh, V. Parvaneh, A. Ehsani, Experimental and

numerical investigation of the generated heat in polypropylene sheet joints using friction stir welding (FSW), International Journal of Material Forming, (2021) 1-17.

[24] H. Aghajani Derazkola, A. Eyvazian, A. Simchi. Submerged friction stir welding of dissimilar joints between an Al-Mg alloy and low carbon steel: Thermo-mechanical modeling, microstructural features, and mechanical properties[J]. Journal of Manufacturing Processes, 2020, 50: 68-79.

[25] W.B. Lee, M. Schmuecker, U.A. Mercardo, et al., Interfacial reaction in steel–aluminum joints made by friction stir welding, Scripta Materialia, 55(4) (2006) 255-358.

[26] FLUENT, Release 2019 R3 - © ANSYS, Inc. All rights reserved.

[27] Z.Z. Yu, W. Zhang, H. Choo, et al., Transient Heat and Material Flow Modeling of Friction Stir Processing of Magnesium Alloy using Threaded Tool, Metallurgical and Materials Transactions A, 43 (2012) 724-737.

[28] G.Q. Chen, Q.Y. Shi, Y.J. Li, et al., Computational fluid dynamics studies on heat generation during friction stir welding of aluminum alloy, Computational Materials Science, 79 (2013) 540–546.

[29] K.C. Mills, Recommended Values of Thermophysical Properties for Selected Commercial Alloys, (2002) 61-65 127-128.

[30] W. Ou, T. Mukherjee, G.L. Knapp, et al., Fusion zone geometries,

cooling rates and solidification parameters during wire arc additive manufacturing, International Journal of Heat and Mass Transfer, 127 (2018) 1084-1094.

[31] P. A.Colegrove, H. R.Shercliff, 3-Dimensional CFD modelling of flow round a threaded friction stir welding tool profile, Journal of Materials Processing Technology, 169 (2) (2005) 320–327.

[32] R. Nandan, G.G. Roy, T. Debroy, Numerical simulation of three-dimensional heat transfer and plastic flow during friction stir welding, Metallurgical and Materials Transactions A, 37 (4) (2006) 1247-1259.

[33] T. Sheppard, A. Jackson, Constitutive equations for use in prediction of flow stress during extrusion of aluminum alloys, Metal Science Journal, 13 (3) (1997) 203-209.

[34] K.E. Tello, A.P. Gerlich, P.F. Mendez, Constants for hot deformation constitutive models for recent experimental data, Sci Technol Weld Join, 15 (3) (2010) 260–266.

[35] G.Q. Chen, Z.L. Feng, Y.C. Zhu, et al., An Alternative Frictional Boundary Condition for Computational Fluid Dynamics Simulation of Friction Stir Welding, Journal of Materials Engineering and Performance, 25 (2016) 4016–4023.

[36] K. Mundra, T. Debroy, K.M. Kelkar2. Numerical Prediction of Fluid Flow and Heat Transfer in Welding with a Moving Heat Source, Numerical Heat Transfer, Part A: Applications, 29 (2) (1996) 115-129.